Hindawi
Advances in Materials Science and Engineering
Volume 2023, Article ID 6588603, 14 pages
https://doi.org/10.1155/2023/6588603

Research Article

Theoretical Investigation of the Nonlinear Optical and Charge Transport Properties of N-(4-Methoxybenzylidene) Isonicotinohydrazone and Some of Its Derivatives: A DFT and TD-DFT Study

Charly Tsapi Tedjeuguim,[1] Stanley Numbonui Tasheh [1,2] and Ghogomu Julius Numbonui [1,2]

[1]*Research Unit of Noxious Chemistry and Environmental Engineering, Department of Chemistry, Faculty of Science, University of Dschang, P.O. Box 67, Dschang, Cameroon*
[2]*Department of Chemistry, Faculty of Science, The University of Bamenda, P.O. Box 39, Bambili, Bamenda, Cameroon*

Correspondence should be addressed to Ghogomu Julius Numbonui; ghogsjuju@hotmail.com

Received 15 July 2022; Revised 26 December 2022; Accepted 28 December 2022; Published 16 January 2023

Academic Editor: Ajay Kumar Mishra

Copyright © 2023 Charly Tsapi Tedjeuguim et al. This is an open access article distributed under the Creative Commons Attribution License, which permits unrestricted use, distribution, and reproduction in any medium, provided the original work is properly cited.

Here, we report the findings from a study on the charge transport and nonlinear optical (NLO) properties of N-(4-methoxybenzylidene) isonicotinohydrazone (INH) and some of its derivatives named INH1-INH15. The density functional theory (DFT) approach was used for ground state computations at the B3LYP-D/6-311G (d,p) level of theory, while the time-dependent density functional theory (TD-DFT) was carried out at the CAM-B3LYP/6-311G (d,p) level. The results show that the energy gaps of all the studied compounds range from 3.933 to 4.645 eV. INH3 and INH4 have the lowest electron and hole reorganization energies (i.e., 0.409 and 0.634 eV, respectively) and can thus be classified as moderate electron and hole-carrying materials for organic light-emitting diode (OLED) applications. TD-DFT computations demonstrate that an extension of the conjugation (in INH2 and INH3) increases the oscillator strength, improving the NLO response. According to the NLO data, INH2 and INH3 have higher static isotropic polarizabilities (38.509 and 37.986×10^{-24} esu, respectively) and second hyperpolarizabilities (54.440 and 57.598×10^{-36} esu, respectively), while INH4 and INH13 have higher first hyperpolarizability values (11.944 and 10.939×10^{-30} esu, respectively). The results reveal that INH derivatives with different groups are viable alternatives for OLED and NLO applications.

1. Introduction

Low molecular weight organic compounds have recently become popular in the optoelectronic industry due to their potential applications in organic light-emitting diodes (OLEDs) [1, 2], organic solar cells (OSCs) [3], organic field effect transistors (OFETs) [4], and nonlinear optics (NGOs) [5–7]. NLO and OLED technologies have received a lot of attention due to their applications in optical and flat-panel displays [8]. Owing to its potential applications in modern computers, optical data storage, communications, laser technology, and photonics, NLO materials have attracted the curiosity of many researchers [9]. Organic compounds containing π-delocalized electrons and push-pull mechanisms have attracted the attention of NLO investigators. Prototypical compounds having NLO features, such as urea and para-nitroaniline (PNA) have such properties [10]. Organic NLO materials are more frequent than their inorganic counterparts due to their affordable fee, low toxicity, ease of solution processability, greater electro-optic coefficients, and flexibility [9, 11, 12]. Despite this, the key challenge in optoelectronic engineering continues to be the development of organic materials with high thermal stability and NLO responsiveness. Designing small novel materials with desirable characteristics will be of interest in optoelectronic engineering.

OLED technology has gained considerable attention as a result of its significance in the development of flat panel displays and lighting, such as those found in smartphones, computers, smartwatches, and televisions [13–15]. Transparency, low thickness, outstanding contrast, good flexibility, viewing angles, lower energy consumption, and faster response time distinguish OLEDs from traditional liquid crystal devices (LCDs) that use a backlighting system [16].

Tris (8-hydroxyquinoline) aluminum complex (Alq_3) is the prototype molecule for the electron transport layer (ETL) in OLEDs [17], while N,N′-diphenyl-N,N′-bis(3-methylphenyl)-1,1′-diphenyl-4,4′-diamine [13] is that for the hole transport layer (HTL). Organic materials do not achieve the same charge carrier mobility as inorganic semiconductors, limiting device efficiency [14, 18]. Developing novel conjugated materials with high mobility and stability is a significant problem in the production of OLED devices.

Owing to their exceptional thermal, optical, and chemical stability, hydrazone compounds have received a great deal of research interest in the past years in the sectors of NLO and OLED technologies [19, 20].

Hentai and collaborators [21] reported that ((1Z)-(4-(dime thylamino) phenyl) methylene) 4-nitrobenzylcarboxyhydrazone monohydrate has a very interesting NLO response. Similarly, Yao and coworkers [22] demonstrated that a class of hydrazone-based photochromic compounds has extremely high hyperpolarizability and can be employed in optoelectronics. Moraes and collaborators [17] discovered that N,N-diisonicotinoyl-2-hydroxy-5-methylisophthalaldehyde hydrazone has intriguing charge transport characteristics. Also, Quirino and colleagues demonstrated that 1-(3-methylphenyl)-1,2,3,4-tetrahydroquinoline-6-carboxaldehyde-1,1′-diphenylhydrazone has excellent hole transport properties and can be employed in optoelectronics [18]. In the same light, Boukabcha and collaborators showed that (Z)-N′-(2, 4-dinitrobenzylidene)-2-quinolinen-8-yloxy) acetohydrazide has a good NLO response and can be employed in optoelectronics [23].

Confronted with microbial resistance-related problems, Kudrat-E-Zahan and coworkers [24] synthesized N-(4-methoxybenzylidene) isonicotinohydrazone (INH) (see Figure 1).

The structural features of this compound with electron delocalization capabilities warrant it to have enhanced NLO responses and charge transport properties. Tedjeuguim and coworkers [25] studied the optoelectronic properties of INH, 2,2′-bipyridine, and their Fe^{2+}, Ni^{2+}, Cu^{2+}, Pd^{2+}, and Pt^{2+} complexes. Unfortunately, there exists no computational studies of the NLO and charge transport properties of INH and its studied derivatives (see Figure 1).

Based on the foregoing, the primary goal of this study is to examine the NLO and charge transport properties of the above-mentioned INH derivatives. To achieve this aim, electronic parameters, UV-spectral analysis, reorganization energies ($\lambda_{\text{electron/hole}}$), mobility ($\mu_{\text{electron/hole}}$), static dipole moment (μ), static polarizability (isotropic ($\langle\alpha\rangle$) and anisotropic ($\Delta\alpha$)), static isotropic first hyperpolarizability (β), and static isotropic second hyperpolarizability (γ) of the studied compounds were computed via the DFT method and are discussed.

2. Computational Details

This study was computed using the Gaussian 09, Revision D.01 program [26]. The GaussView 6.0.16 program was used to visualize and build the investigated compounds [27]. Geometry optimizations and frequency calculations were performed using Becke's three Lee-Yang-Parr (B3LYP) functional [28] augmented with an empirical dispersion term [29] and associated with the Pople style 6-311G (d,p) basis set [30]. B3LYP was used because it is suitable for predicting the optoelectronic properties of low molecular weight organic molecules [31]. The excited singlet state structures were computed using the TD-DFT/CAM-B3LYP/6-311G (d,p) method, which has proven to be effective in determining the charge transfer transition energies of low molecular weight organic molecules [32].

Experimental results of INH (IR and UV spectra) were reported by Kudrat-E-Zahan and coworkers [24]. IR analysis shows that INH displays characteristic bands at 1658.84 and 1598.69 cm^{-1} assigned to ν(C=O) and ν(C=N) vibrations, respectively. Theoretically, the ν(C=O) and ν(C=N) bonds of INH vibrate at 1711.40 and 1600.77 cm^{-1}, respectively. The calculated frequencies were scaled by a factor of 0.99 per the B3LYP-D/6-311G (d,p) level of theory and show good agreement with the experimental results. UV analysis shows that the computed λ_{abs} value of INH is 268.39 nm and also shows good agreement with the experimental value (283 nm) [24]. In this work, the electronic properties, nonlinear optical and charge transport properties of the studied compounds were calculated at B3LYP-D/6-311G (d,p) level of theory in the gaseous phase.

According to Koopman's theorem [33], frontier molecular orbital parameters such as band gap (ΔE_g), chemical potential (μ), chemical hardness (η), chemical softness (S), electrophilicity (ω), and the maximum transferred charge ($\Delta N_{\max}$) were evaluated according to equations (1)–(6), respectively,

$$\Delta E_{\text{g}} = E_{\text{LUMO}} - E_{\text{HOMO}}, \tag{1}$$

$$\mu = \frac{(E_{\text{LUMO}} + E_{\text{HOMO}})}{2}, \tag{2}$$

$$\eta = \frac{(E_{\text{LUMO}} - E_{\text{HOMO}})}{2}, \tag{3}$$

$$S = \frac{1}{2\eta}, \tag{4}$$

$$\omega = \frac{\mu^2}{2\eta}, \tag{5}$$

$$\Delta N_{\max} = \frac{-\mu}{\eta}. \tag{6}$$

The charge transport properties of organic materials can be studied using many parameters such as the reorganization energy ($\lambda_{\text{electron/hole}}$), charge transfer integral ($t_{\text{electron/hole}}$), mobility ($\mu_{\text{electron/hole}}$), charge transport rate ($k_{\text{electron/hole}}$),

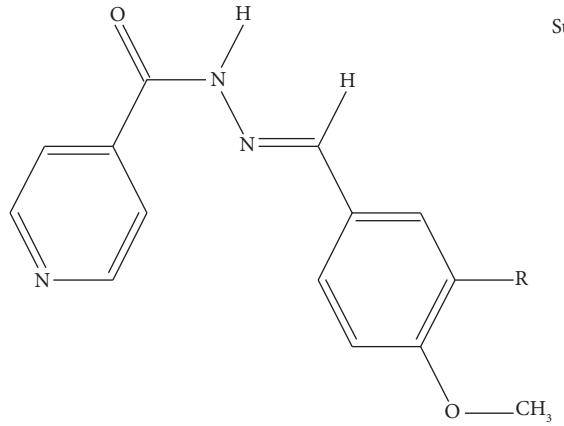

Substituent (R)	Compounds
–H	INH
$-CH_3$	INH1
$-C_6H_5$	INH2
$-C_4H_3S$	INH3
–SH	INH4
–F	INH5
–Cl	INH6
–Br	INH7
$-NO_2$	INH8
–CHO	INH9
–COOH	INH10
$-OCH_3$	INH11
–OH	INH12
$-NH_2$	INH13
–CN	INH14
$-NMe_2$	INH15

Figure 1: Structural representation of N-(4-methoxybenzylidene) isonicotinohydrazone (INH) and its studied derivatives.

adiabatic ionization potential (IP_a), and adiabatic electron affinity (EA_a). The charge transport rate is one of the key parameters governing the performance of organic electronic devices [34]. It has been extensively used to describe the charge transfer mechanism in many organic materials at room temperature and presents a good agreement with experiment [35]. The charge transport rate can be obtained through Marcus's theory [36] and is calculated according to (7)as follows:

$$k_{\text{electron/hole}} = \frac{4\pi^2}{h} \frac{1}{\sqrt{4\pi K_B T \lambda_{\text{electron/hole}}}} t^2_{\text{electron/hole}} \exp\left(-\frac{\lambda_{\text{electron/hole}}}{4K_B T}\right), \tag{7}$$

where $\lambda_{\text{electron/hole}}$ is the reorganization energy of the electron or the hole, $t_{\text{electron/hole}}$ is the integral charge transfer of the electron or the hole, k_B is the Boltzmann constant ($1.380 \times 10^{-23}\,\text{JK}^{-1}$), h is Planck's constant ($6.626 \times 10^{-34}\,\text{Js}$), and T is the temperature (298.15 K). High temperatures are known to limit Marcus's theory [37].

Reorganization energy is partitioned into internal and external reorganization energies [8]. The internal reorganization energy refers to the energy change of the system caused by the structural relaxation after the gain or loss of electrons, while the external reorganization energy describes the change in electronic polarization of the surrounding compounds [38, 39]. The external reorganization energy contribution is usually neglected owing to the fact that their energies are much smaller than those of their internal counterparts [39, 40]. Reorganization energy is the parameter that affects the charge transport rate (K) of materials. Lower electron ($\lambda_{\text{electron}}$) and hole ($\lambda_{\text{hole}}$) reorganization energies are beneficial for higher electron and hole transport rates, respectively [41]. The reorganization energy of electrons and holes was calculated using the following equations:

$$\begin{aligned} \lambda_{\text{electron}} &= \left(E_0^- - E_-^-\right) + \left(E_-^0 - E_0^0\right), \\ \lambda_{\text{hole}} &= \left(E_0^+ - E_+^+\right) + \left(E_+^0 - E_0^0\right), \end{aligned} \tag{8}$$

where $E_0^+ (E_0^-)$ indicates the energy of the cation (anion) calculated from the optimized geometry of the neutral compound, $E_+^+ (E_-^-)$ represents the energy of the cation (anion) computed from the optimized structure of the cationic and anionic forms of the compound, respectively; $E_+^0 (E_-^0)$ is the energy of neutral molecules calculated based on the optimized structures of the cationic and anionic states of the molecule, respectively, while E_0^0 is the energy of the neutral compound computed from the optimized structure of the neutral compound.

Another controlling factor to assess the charge transport of compounds is the charge transfer integral (t) [42]. It is directly related to frontier molecular orbitals (highest occupied molecular orbital (HOMO) and lowest unoccupied molecular orbital (LUMO) energy) in the dimer configuration [43]. Charge transfer integral (t) is evaluated using Koopman's theorem (KT) according to the following equations:

$$\begin{aligned} t_{\text{electron}} &= \frac{1}{2}\left(E_{\text{LUMO+1}} - E_{\text{LUMO}}\right), \\ t_{\text{hole}} &= \frac{1}{2}\left(E_{\text{HOMO}} - E_{\text{HOMO-1}}\right). \end{aligned} \tag{9}$$

Charge mobility is another parameter that affects the performance of OLED materials. High charge carrier mobility is enhanced by high charge transfer integral and low reorganization energies. The charge mobility is given by Einstein's equation [43] as follows:

$$\mu_{\text{electron/hole}} = \frac{ed^2 K_{\text{electron/hole}}}{2K_B T}, \tag{10}$$

where $K_{\text{electron/hole}}$ is the charge transport rate for the hole or electron, K_B is the Boltzmann constant, d is the intermolecular distance between two monomers, e is the electronic charge, and T is the temperature at 298.15 K.

Ionization potentials (IPs) and electron affinities (EAs) describe the charge transport properties of OLED materials [5]. A smaller IP and greater EA value lead to the effective hole and electron injection ability [44]. The adiabatic ionization potential (IP_a), vertical ionization potential (IP_v), adiabatic electron affinity (EA_a), and vertical electron affinity (EA_V) in this work were calculated as follows:

$$\begin{aligned} \text{IP}_a &= E_+^+ - E_0^0, \\ \text{IP}_v &= E_0^+ - E_0^0, \\ \text{EA}_a &= E_0^0 - E_-^-, \\ \text{EA}_V &= E_0^0 - E_0^-. \end{aligned} \tag{11}$$

Stability is a beneficial parameter for the charge transport of organic materials [39]. Good OLED devices are those with larger chemical stabilities. The absolute hardness (η) was calculated to estimate the stability of the organic materials using the following equation [38]:

$$\eta = \frac{\text{IP}_a - \text{EA}_a}{2}. \tag{12}$$

To assess the possibility of INH and its derivatives as potential NLO materials, the static dipole moment (μ), static isotropic ($\langle\alpha\rangle$) and anisotropic ($\Delta\alpha$) polarizability, static isotropic first hyperpolarizability (β), and static isotropic second hyperpolarizability (γ) were calculated. Values were computed at x, y, and z components using the following equations [45, 46]:

$$\begin{aligned} \mu &= \sqrt{\left(\mu_x^2 + \mu_y^2 + \mu_z^2\right)}, \\ \langle\alpha\rangle &= \frac{1}{3}\left(\alpha_{xx} + \alpha_{yy} + \alpha_{zz}\right), \\ \Delta\alpha &= \frac{1}{\sqrt{2}}\left[\left(\alpha_{xx} - \alpha_{yy}\right)^2 + \left(\alpha_{yy} - \alpha_{zz}\right)^2 + \left(\alpha_{zz} - \alpha_{xx}\right)^2 + 6\left(\alpha_{xy}^2 + \alpha_{xz}^2 + \alpha_{yz}^2\right)\right], \\ \beta_{\text{total}} &= \left(\beta_x^2 + \beta_y^2 + \beta_z^2\right)^{1/2}, \end{aligned} \tag{13}$$

where

$$\begin{aligned} \beta_x &= \beta_{xxx} + \beta_{xyy} + \beta_{xzz}, \\ \beta_y &= \beta_{yyy} + \beta_{xxy} + \beta_{yzz}, \\ \beta_z &= \beta_{zzz} + \beta_{xxz} + \beta_{yyz}, \end{aligned} \tag{14}$$

with $\beta_x, \beta_y,$ and β_z known, equation (13) becomes the following equation:

$$\beta_{\text{total}} = \left[\left(\beta_{xxx} + \beta_{xyy} + \beta_{xzz}\right)^2 + \left(\beta_{yyy} + \beta_{xxy} + \beta_{yzz}\right)^2 + \left(\beta_{zzz} + \beta_{xxz} + \beta_{yyz}\right)^2\right]^{1/2}, \tag{15}$$

where β_{xxx}, β_{xyy}, β_{xzz}, β_{yyy}, β_{xxy}, β_{yzz}, β_{zzz}, β_{xxz}, and β_{yyz} are the tensor components for the first hyperpolarizability.

$$\gamma = \frac{1}{5}\left[\gamma_{xxxx} + \gamma_{yyyy} + \gamma_{zzzz} + 2\left(\gamma_{xxyy} + \gamma_{xxzz} + \gamma_{yyzz}\right)\right], \tag{16}$$

where γ_{xxxx}, γ_{yyyy}, γ_{zzzz}, γ_{xxyy}, γ_{xxzz}, and γ_{yyzz} are the fourth-order tensor components of the second hyperpolarizability. A compound with a large dipole moment and hyperpolarizability value is predicted to be a potential candidate for NLO response [46].

3. Results and Discussion

3.1. Frontier Molecular Orbital Analysis. Frontier molecular orbitals were calculated from DFT-based optimized structures using the equations specified in the computational details section. Table 1 presents the electronic parameters of N-(4-methoxybenzylidene) isonicotinohydrazone and its derivatives.

The results show that functionalization of a donor at the terminal of N-(4-methoxybenzylidene) isonicotinohydrazone induces a reduction in the energy gap of INH (see INH1, INH4, INH11, INH12, INH13, and INH15). Similarly,

Table 1: Electronic parameters of N-(4-methoxybenzylidene) isonicotinohydrazone and its derivatives calculated at B3LYP-D/6-311G (d,p) level of theory in the gaseous phase.

Compounds	E_H[a]	E_L[a]	ΔE_g[a]	μ[a]	η[a]	S[b]	ω[a]	ΔN_{max}
INH	−6.341	−1.918	4.423	−4.129	2.211	0.226	3.854	1.867
INH1	−6.226	−1.902	4.324	−4.064	2.162	0.231	3.819	1.879
INH2	−6.500	−1.991	4.509	−4.245	2.254	0.221	3.996	1.883
INH3	−6.358	−2.022	4.336	−4.190	2.168	0.230	4.048	1.932
INH4	−6.256	−1.986	4.270	−4.121	2.135	0.234	3.977	1.930
INH5	−6.456	−2.045	4.411	−4.250	2.205	0.226	4.094	1.927
INH6	−6.817	−2.176	4.641	−4.496	2.320	0.215	4.355	1.937
INH7	−6.812	−2.167	4.645	−4.489	2.322	0.215	4.338	1.933
INH8	−6.852	−2.919	3.933	−4.885	1.966	0.254	6.067	2.484
INH9	−6.640	−2.378	4.262	−4.509	2.131	0.234	4.770	2.115
INH10	−6.589	−2.115	4.474	−4.352	2.237	0.223	4.233	1.945
INH11	−6.334	−1.966	4.368	−4.150	2.184	0.228	3.942	1.900
INH12	−6.239	−1.923	4.316	−4.081	2.158	0.231	8.858	1.891
INH13	−5.830	−1.822	4.008	−3.826	2.004	0.249	3.652	1.909
INH14	−6.755	−2.230	4.525	−4.492	2.262	0.220	4.459	1.985
INH15	−6.071	−1.929	4.142	−4.000	2.071	0.241	3.862	1.931

$E_H \longrightarrow$ HOMO energy, $E_L \longrightarrow$ LUMO energy, $\Delta E_g \longrightarrow$, $\mu \longrightarrow$ chemical potential, $\eta \longrightarrow$ chemical hardness, $\omega \longrightarrow$ electrophilicity index, $\Delta N_{max} \longrightarrow$ the maximum transferred charge, [a]units in eV, and [b]units in eV^{-1}.

functionalization with an acceptor only raises the band gap in the other cases and decreases it in INH8. Thus, compounds with small band gaps are softer, more reactive, and can show excellent NLO response [47]. The band gaps of all the studied compounds are in the range of 3.933 to 4.645 eV. This reduction in the energy gap of the designed derivatives compared to the synthesized (N-(4-methoxybenzylidene) isonicotinohydrazone) compound is attributed to the introduction of suitable donor and acceptor substituents. Hardness is the ability to resist charge transfer within its environment. The hardness values of all the investigated compounds range from 1.966 to 2.322 eV. Among these compounds, INH8 has the lowest hardness value (1.966 eV) and is therefore the most reactive. Organic materials with high and positive ω and ΔN_{max} values have a greater affinity to absorb an electron. However, if a compound has a low amount of these indices, it may be characterized as an electron donor [48]. The maximum transferred charge (ΔN_{max}) and electrophilicity index (ω) values for all investigated compounds are positive and are in the range of 1.867 to 2.484 eV and 3.652 to 8.858 eV, respectively. The highest ΔN_{max} value of INH8 (2.484 eV) suggests that this compound has a greater tendency to absorb an electron. Based on the ongoing, INH8 is the most reactive compound and has the highest tendency to absorb an electron.

Figure 2 shows the HOMO and LUMO distributions of all the investigated compounds.

The results show that the HOMOs are distributed on the $-OCH_3$ group and the benzene ring of all the studied compounds. The LUMOs, on their part, are located on the pyridine ring of all the studied compounds except INH2, INH3, INH8, and INH9.

3.2. Molecular Electrostatic Potential (MEP) Map. The molecular electrostatic potential (MEP) map is a crucial parameter for describing the electrophilic and nucleophilic centres of a system [49]. On the colour-coded surfaces, the blue region shows the area of low electron density (i.e., the regions of positive potential), while the red region indicates the area of high electron density (i.e., regions of negative potential) [50–52]. Displayed in Figure 3 are the MEP plots of the compounds under investigation.

These findings show that the red electron-rich sites are centred on the oxygen atom of the carbonyl, the nitrogen atom of the pyridine ring, and the nitrogen atom of the azomethine group in all the studied compounds. In contrast, the blue electron-deficient sites are predominantly on the protons of the azomethine and methoxyl groups (except for INH2, INH3, INH7, and INH15).

3.3. Reorganization Energies. Presented in Table 2 are important parameters needed to understand the charge transport nature and charge injection.

Small reorganization ($\lambda_{electron/hole}$) energy values indicate better charge transport rates and mobility, which give rise to good charge transport properties for the materials [39]. Results from Table 2 show that the increasing trend in the $\lambda_{electron}$ values is as follows: INH3 < INH9 < INH2 < INH < INH6 = INH5 < INH1 < INH15 < INH4 < INH11 < INH12 < INH14 < INH5 < INH12 < INH13 < INH8. This implies that INH3 (0.409 eV) possesses the best electron transport properties, while INH8 (0.703 eV) has the least. Moreover, the increasing trend in λ_{hole} values is as follows: INH4 < INH15 < INH3 < INH12 < INH13 < INH1 < INH5 < INH14 < INH < INH9 < INH2 < INH8 < INH11 < INH10 < INH7 < INH6. This suggests that INH4 (0.634 eV) possesses the best hole transport properties, while INH6 (1.197 eV) has the least. The results also show that the $\lambda_{electron}$ values are relatively smaller than those of the λ_{hole} values. This illustrates the potential of the studied compounds as n-type materials for organic light-emitting devices.

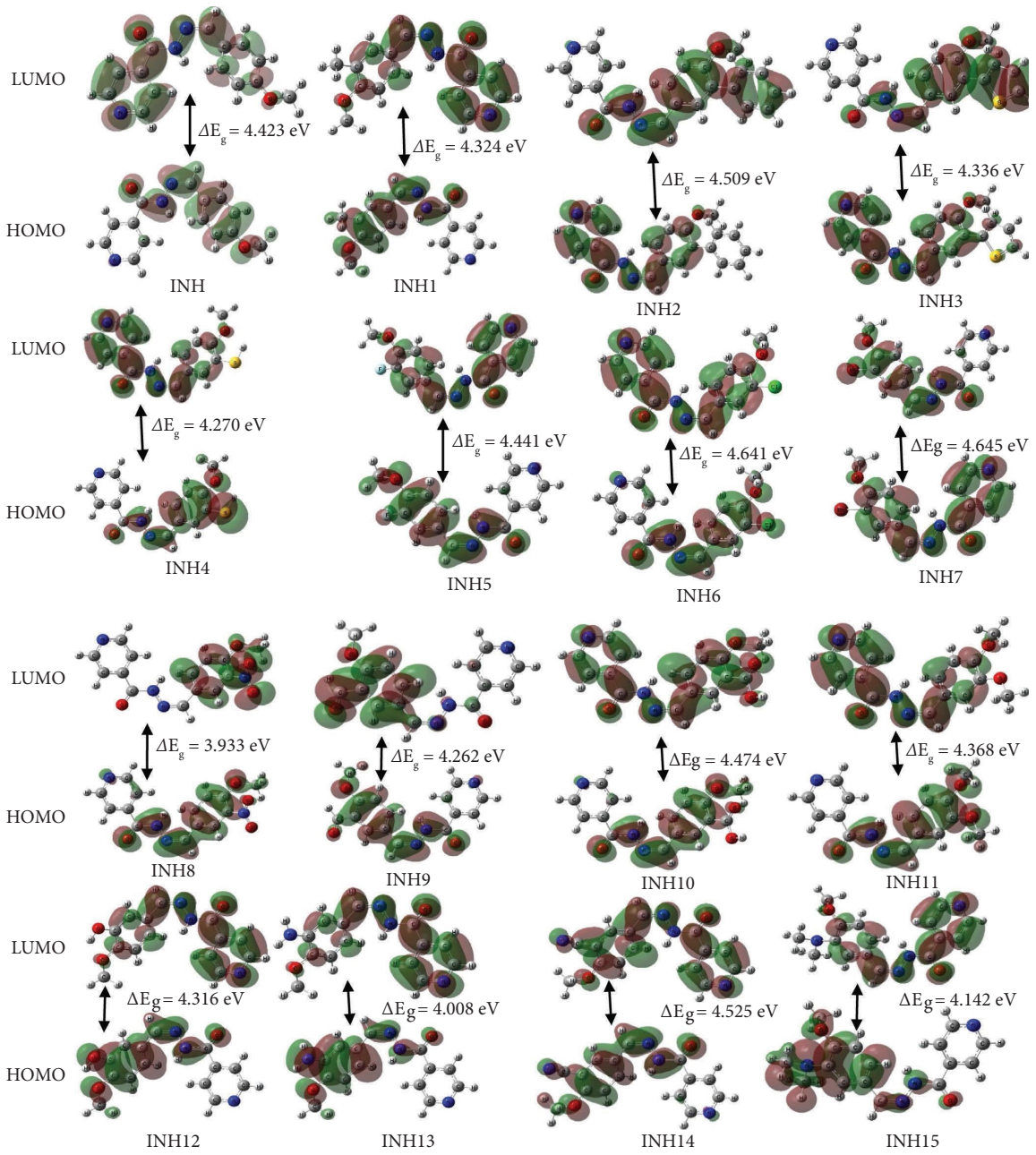

Figure 2: Representation of the HOMOs and LUMOs of the studied compounds as calculated at B3LYP-D/6-311G (d,p) level of theory in the gaseous phase.

A smaller IP_a value means easier hole injection ability for the OLED materials, while a larger EA_a value facilitates electron injection [8, 53]. Table 2 shows that INH13 (7.129 eV) has the lowest IP_a value, while INH8 (1.578 eV) has the highest EA_a value. The results also indicate that INH1 is the most stable compound under investigation, with the highest η value (3.702 eV). Good charge transporters for high-performance OLED devices are those with high thermal and chemical stabilities. Thus, the stability of our compounds follows the order: INH8 < INH15 < INH11 < INH10 < INH13 = INH3 < INH2 < INH9 < INH14 < INH7 < INH6 = INH5 = INH4 < INH < INH12 < INH1. Based on the above analyses, the functionalization of N-(4-methoxybenzylidene) isonicotinohydrazone using donor and acceptor groups enhances the performance of the materials in some cases.

3.4. Charge Transfer Integrals, Charge Transport Rate, and Mobility of the Studied Compounds. Presented in Table 3 are the charge transfer integrals, charge transport rate, and mobility values of the studied compounds. These values were computed using the intermolecular distance of 4.0 Å between the two monomers.

Large charge transfer integral values improve the mobility and conductivity of OLED materials [16]. The findings in Table 3 show that the $t_{electron}$ ranges from 0.012 to

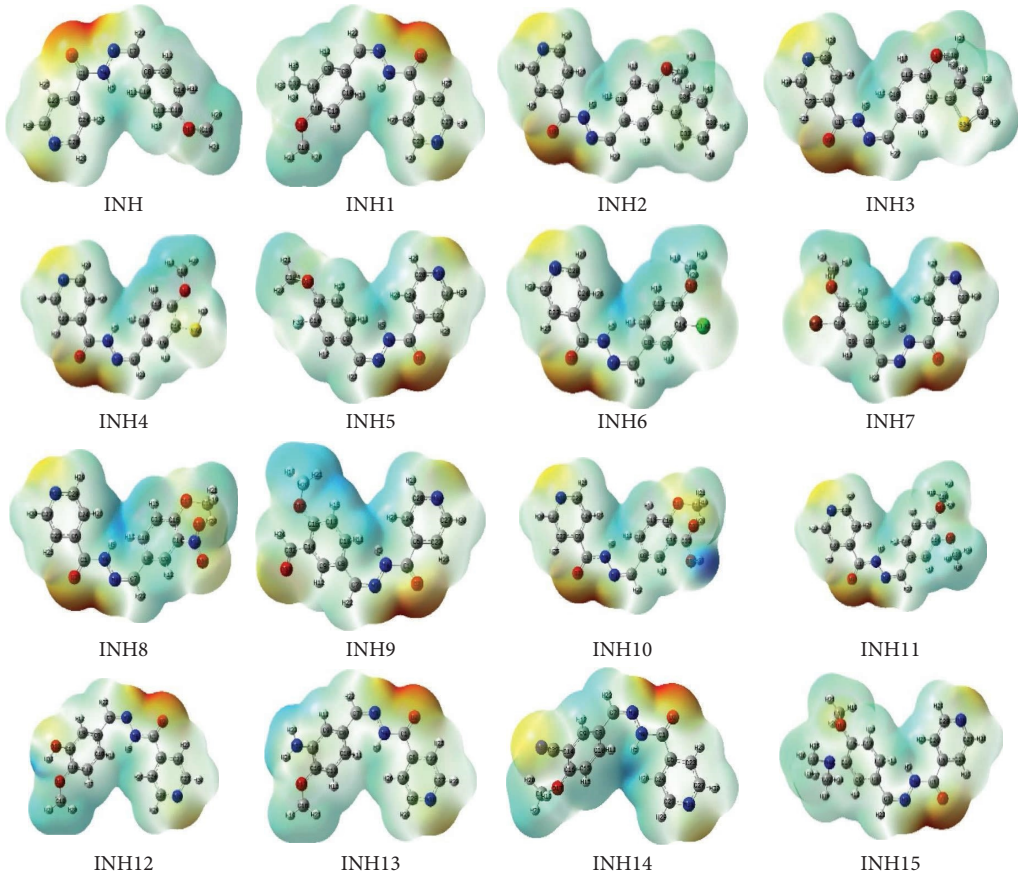

Figure 3: Molecular electrostatic potential plots of the compounds under investigation, calculated at the B3LYP-D/6-311G (d,p) level of theory in the gaseous phase.

Table 2: Reorganization energies, adiabatic electron affinity, vertical electron affinity, vertical ionization potential, adiabatic ionization potential, and hardness of the studied compounds all in eV, computed at the B3LYP-D/6-311G (d,p) level of theory in the gaseous phase.

Compounds	IP_a	EA_a	IP_V	EA_V	η	$\lambda_{electron}$	λ_{hole}
INH	7.510	0.653	7.918	0.408	3.428	0.480	0.918
INH1	7.428	0.653	7.809	0.408	3.702	0.489	0.859
INH2	7.456	0.870	7.891	0.625	3.293	0.440	0.963
INH3	7.483	0.925	7.755	0.680	3.279	0.409	0.707
INH4	7.510	0.761	7.782	0.517	3.374	0.494	0.634
INH5	7.619	0.870	8.027	0.707	3.374	0.578	0.890
INH6	7.728	0.979	8.354	0.707	3.374	0.488	1.197
INH7	7.728	1.006	0.286	0.707	3.361	0.488	1.181
INH8	7.918	1.578	8.354	1.197	3.169	0.703	0.992
INH9	7.728	1.115	0.300	0.032	3.306	0.415	0.955
INH10	7.646	1.088	7.864	0.734	3.278	0.579	1.007
INH11	7.292	0.761	7.864	0.489	3.265	0.495	0.995
INH12	7.864	0.680	7.809	0.408	3.592	0.511	0.802
INH13	7.129	0.571	7.456	0.299	3.279	0.584	0.845
INH14	7.864	1.197	8.272	0.816	3.333	0.563	0.908
INH15	7.265	0.740	7.592	0.473	3.262	0.491	0.644

Note. $\lambda_{electron/hole}$: reorganization energies, EA_a: adiabatic electron affinity, EA_V: vertical electron affinity, IP_V: vertical ionization potential, IP_a: adiabatic ionization potential, and η: hardness.

0.346 eV, while the t_{hole} varies from 0.019 to 0.538 eV. INH is found to have the highest electron transport rate with a value of $2.566 \times 10^{13}\ s^{-1}$. This leads to an increase in the mobility of electron transport with a value of $7.982 \times 10^{-1}\ cm^2V^{-1}s^{-1}$ and can be used for OLED-based applications. The results in the table also show that the electron mobility values of the different compounds follow the trend: INH > INH9 > INH12 > INH4 > INH2 > INH1 > INH8 > INH11 > INH7 >

Table 3: The charge transfer integrals, charge transport rates, and mobilities of the molecules studied compounds, computed at the B3LYP-D/6-311G (d,p) level of theory in the gaseous phase.

Compounds	$t_{electron}$[a]	t_{hole}[a]	$k_{electron}$[b]	k_{hole}[b]	$\mu_{electron}$[c]	μ_{hole}[c]
INH	0.336	0.344	2.566×10^{13}	2.752×10^{11}	7.982×10^{-1}	8.561×10^{-3}
INH1	0.128	0.159	3.381×10^{12}	1.078×10^{11}	1.051×10^{-1}	3.353×10^{-3}
INH2	0.117	0.512	4.795×10^{12}	3.843×10^{11}	1.491×10^{-1}	1.195×10^{-2}
INH3	0.048	0.313	1.131×10^{12}	2.019×10^{12}	3.518×10^{-2}	6.281×10^{-2}
INH4	0.202	0.019	7.980×10^{12}	1.597×10^{10}	2.482×10^{-1}	4.968×10^{-4}
INH5	0.115	0.252	1.056×10^{12}	1.969×10^{11}	3.285×10^{-2}	6.125×10^{-3}
INH6	0.023	0.121	1.103×10^{11}	1.979×10^{9}	3.431×10^{-3}	6.156×10^{-5}
INH7	0.101	0.063	2.128×10^{12}	6.311×10^{8}	6.620×10^{-2}	1.963×10^{-5}
INH8	0.346	0.441	2.573×10^{12}	3.178×10^{11}	8.004×10^{-2}	9.886×10^{-3}
INH9	0.212	0.432	2.067×10^{13}	2.970×10^{11}	6.430×10^{-1}	9.239×10^{-3}
INH10	0.046	0.028	1.673×10^{11}	7.329×10^{8}	5.204×10^{-3}	2.280×10^{-5}
INH11	0.105	0.157	2.133×10^{12}	2.604×10^{10}	6.635×10^{-2}	8.100×10^{-4}
INH12	0.341	0.026	1.895×10^{13}	5.195×10^{9}	5.895×10^{-1}	1.616×10^{-4}
INH13	0.110	0.148	9.073×10^{11}	1.079×10^{11}	2.822×10^{-2}	3.356×10^{-3}
INH14	0.012	0.092	1.348×10^{10}	2.181×10^{10}	4.193×10^{-4}	6.785×10^{-4}
INH15	0.090	0.538	1.636×10^{12}	1.153×10^{13}	5.089×10^{-2}	3.586×10^{-1}

Note. $t_{electron}/t_{hole}$ ⟶ charge transfer integral of the electron or hole, $k_{electron}/k_{hole}$ ⟶ charge transport rate of the electron or hole, $\mu_{electron}/\mu_{hole}$ ⟶ mobility of the electron or hole, [a]in eV, [b]in s^{-1}, and [c]in $cm^2V^{-1}s^{-1}$.

INH15 > INH5 > INH3 > INH13 > INH10 > INH6 > INH14.

The results also indicate that INH15 has the highest hole transport rate ($1.153\times10^{13}\,s^{-1}$) as compared to the others. The increase in this value also leads to an increase in the hole transport mobility with a value of $3.586\times10^{-1}\,cm^2V^{-1}s^{-1}$ and can be used in OLED technology. Moreover, the hole mobility values of the different compounds decrease as follows: INH15 > INH3 > INH2 > INH8 > INH9 > INH > INH5 > INH13 > INH1 > INH11 > INH14 > NH4 > INH12 > INH6 > INH10 > INH7. In the present work, the electron transfer integral and charge mobility of the studied compounds are generally higher than their hole transfer integral and charge mobility. So, it can be said that the series of N-(4-methoxybenzylidene) isonicotinohydrazone derivatives are good candidates for electron transfer material and charge mobility in OLED technology.

3.5. UV Spectral Analyses via TD-DFT. The UV absorption spectra of the studied compounds were evaluated. The first 10 excited states were calculated at the CAM-B3LYP/6-311G (d, p) level of theory. The calculated absorption wavelength (λ_{abs}), excitation energy (E_{abs}), oscillator strength, and orbital coefficients are summarized in Table 4. It is worth mentioning that only the oscillator strengths of the most intense bands are presented.

The result shows that the oscillator strengths range from 0.270 to 0.520. The most intense absorption band was recorded for compound INH2 with an oscillator strength of 0.520. The findings also show that the oscillator strength increases upon the extension of the conjugation system (see INH2 and INH3). The wavelengths of the investigated compounds are found to range from 216.06 to 273.64 nm. Generally, the functionalization of INH is found to reduce the wavelengths of the studied compounds except for INH1 and INH5. The computed λ_{abs} value of N-(4-methoxybenzylidene) isonicotinohydrazone is 268.39 nm and shows good agreement with the experimental value of 283 nm [24].

The absorption energies are in the range of 4.531 to 5.738 eV. Functionalization of INH is observed to enhance the energy of the studied compounds except for INH1 and INH5. The shorter wavelengths and higher energies show that the investigated compounds are attributed to $\pi-\pi^*$ transitions. Lower transition energies accompanied by higher oscillator strength will lead to a greater charge transfer, which consecutively results in robust NLO response (second hyperpolarizability) properties [47]. The recorded UV-Vis absorption spectra of the studied compounds are presented in the supplementary information (SI) file. The peaks at longer wavelength regions (lower energy) are associated with intramolecular charge transfer (ICT), whereas $\pi-\pi^*$ transitions appear in the shorter wavelength regions (higher energy) [54].

3.6. Nonlinear Optical Properties. Organic molecules are gaining importance in nonlinear optics as they exhibit good NLO activities because of extendable π-conjugation and the ease of functionalization of a donor and an acceptor at the terminals of a conjugated molecular system [55]. The NLO properties such as static dipole moment (μ), static isotropic ($\langle\alpha\rangle$) and anisotropic ($\Delta\alpha$) polarizability, static isotropic first hyperpolarizability (β), and static isotropic second hyperpolarizability (γ) of the studied compounds are reported in Tables 5–8, respectively. The above-mentioned tensor components were recorded in atomic units (a.u) and converted into electrostatic units (esu) using the conversion factors: 1 a.u. = 0.15×10^{-24} esu for polarizability (α_{static}), 1 a.u = 8.6393×10^{-33} esu for first hyperpolarizability (β_{static}), and 1 a.$u = 0.50367\times10^{-39}$ esu for second hyperpolarizability ($\gamma_{stactic}$) [56].

Table 4: Excitation energies, wavelengths, oscillator strengths, molecular orbitals, and dominant electronic transitions of the studied compounds obtained at the CAM-B3LYP/6-311G (d,p) level of theory in the gaseous phase.

Compounds	Excited state	MO + coefficient	E_{abs}	λ_{abs}	f
INH	$S_0 \longrightarrow S_2$	H ⟶ L (48%)	4.610	268.39	0.370
INH1	$S_0 \longrightarrow S_5$	H ⟶ L (50%)	4.531	273.64	0.270
INH2	$S_0 \longrightarrow S_5$	H⟶L + 1 (42%)	5.178	239.42	0.520
INH3	$S_0 \longrightarrow S_4$	H − 1 ⟶ L (49%)	4.769	259.95	0.432
INH4	$S_0 \longrightarrow S_{10}$	H − 1 ⟶ L + 1 (32%)	5.592	221.72	0.329
INH5	$S_0 \longrightarrow S_2$	H ⟶ L (39%)	4.597	269.70	0.276
INH6	$S_0 \longrightarrow S_2$	H ⟶ L (58%)	4.683	264.72	0.410
INH7	$S_0 \longrightarrow S_2$	H ⟶ L (58%)	4.692	264.20	0.411
INH8	$S_0 \longrightarrow S_5$	H ⟶ L + (57%)	4.663	265.87	0.478
INH9	$S_0 \longrightarrow S_4$	H ⟶ L + 1 (53%)	4.701	263.70	0.445
INH10	$S_0 \longrightarrow S_3$	H ⟶ L + 1 (46%)	4.705	263.47	0.426
INH11	$S_0 \longrightarrow S_9$	H − 1 ⟶ L(38%)	5.738	216.06	0.329
INH12	$S_0 \longrightarrow S_1$	H − 1 ⟶ L (40%)	5.709	217.15	0.354
INH13	$S_0 \longrightarrow S_9$	H − 1⟶L (32%)	5.506	225.14	0.298
INH14	$S_0 \longrightarrow S_3$	H ⟶ L + 1 (43%)	4.685	264.61	0.445
INH15	$S_0 \longrightarrow S_5$	H ⟶ L + 2 (38%)	5.103	242.96	0.344

Note. E_{abs}: excitation energies (in eV), λ_{abs}: wavelengths (in nm), f: oscillator strengths, MO: molecular orbital coefficients, H: HOMO, and L: LUMO.

Table 5: The static electric dipole moment (μ) of the studied compounds, calculated at $\omega = 0$ at B3LYP-D/6-311G (d,p) level of theory in the gaseous phase.

Species	μ_x	μ_y	μ_z	μ_{static} (a.u)	μ_{static} (debye)
INH	1.611	0.364	−2.292	2.825	7.181
INH1	1.027	−0.225	−2.456	2.672	6.792
INH2	1.692	−0.085	−1.979	2.605	6.623
INH3	1.531	−0.076	−2.113	2.611	6.636
INH4	0.000	0.000	2.678	2.678	6.807
INH5	1.082	0.169	−2.022	2.300	5.847
INH6	0.268	0.153	−1.643	1.672	4.250
INH7	0.000	0.000	1.692	1.692	4.302
INH8	0.572	−1.015	−1.425	1.841	4.680
INH9	0.000	0.000	2.737	2.737	6.957
INH10	1.605	−0.160	−1.501	2.203	5.601
INH11	1.442	0.973	−1.716	2.444	6.212
INH12	0.759	−0.521	−2.820	2.966	7.540
INH13	1.624	−0.198	−2.651	3.115	7.919
INH14	0.180	−0.615	−1.679	1.797	4.569
INH15	1.515	0.772	−2.078	2.685	6.825

Table 6: Static average polarizabilities of the studied compounds, calculated at $\omega = 0$ at the B3LYP-D/6-311G (d, p) level of theory in the gaseous phase.

Species	α_{xx}	α_{xy}	α_{yy}	α_{xz}	α_{yz}	α_{zz}	$\langle\alpha\rangle$ (a.u)	$\langle\alpha\rangle \times 10^{-24}$ esu	$\Delta\alpha$ (a.u)	$\Delta\alpha \times 10^{-24}$ esu
INH	233.247	8.5703	104.8420	−45.129	15.1361	232.0130	190.034	28.161	152.802	22.643
INH1	246.245	13.452	119.00	−41.579	19.576	243.558	202.934	30.071	150.784	22.343
INH2	325.528	43.596	171.007	−59.578	−13.183	283.082	259.872	38.509	189.714	28.112
INH3	315.087	4.780	170.133	−58.606	−9.602	283.879	256.366	37.989	186.809	27.682
INH4	237.661	−34.605	128.491	38.609	−24.876	266.467	210.873	31.248	160.667	23.808
INH5	234.487	9.672	104.145	−45.272	13.797	233.287	190.640	28.249	154.385	22.877
INH6	244.880	20.954	117.990	−41.378	4.469	235.346	199.405	29.548	146.615	21.726
INH7	236.591	−22.178	125.609	45.0165	7.842	255.322	205.841	30.502	149.954	22.220
INH8	254.826	16.177	121.556	−49.102	14.430	243.722	206.701	30.630	158.263	23.452
INH9	253.230	−37.503	128.743	27.027	−31.849	233.080	205.018	30.380	151.158	22.399
INH10	254.298	19.375	127.220	−5.234	14.372	246.456	209.325	31.018	158.679	23.513
INH11	254.876	22.234	124.974	−40.048	5.154	240.648	206.833	30.649	146.981	21.780

Table 6: Continued.

Species	α_{xx}	α_{xy}	α_{yy}	α_{xz}	α_{yz}	α_{zz}	$\langle\alpha\rangle$ (a.u)	$\langle\alpha\rangle \times 10^{-24}$ esu	$\Delta\alpha$ (a.u)	$\Delta\alpha \times 10^{-24}$ esu
INH12	233.607	11.929	110.391	−38.917	19.621	235.560	193.186	28.627	146.807	21.755
INH13	243.889	17.250	115.908	−42.243	17.463	240.765	200.187	29.664	152.152	22.546
INH14	257.878	23.986	121.423	−54.016	9.002	242.381	207.228	30.708	165.735	24.559
INH15	281.330	23.955	138.409	−47.487	3.358	255.100	224.946	33.333	160.891	23.842

$\langle\alpha\rangle$: isotropic polarizability and Δ_α: anisotropic polarizability.

Table 7: Static first hyperpolarizability of the studied compounds, calculated at $\omega = 0$, at the B3LYP-D/6-311G (d,p) level of theory in the gaseous phase.

Compounds	β_x	β_y	β_z	β_{static} (a.u)	$\beta_{static} \times 10^{-30}$ esu
INH	−683.005	187.200	785.031	1057.26	9.130
INH1	−849.400	72.728	808.772	1175.109	10.152
INH2	−631.867	−112.204	465.456	792.776	6.849
INH3	−846.022	−360.898	625.3536	1112.235	9.608
INH4	−850.633	411.624	−1009.242	1382.599	11.944
INH5	−780.196	94.948	885.191	1183.758	10.226
INH6	−586.197	25.427	289.774	654.402	5.653
INH7	−563.781	−19.462	−236.9632	611.865	5.286
INH8	−183.556	241.853	353.656	466.109	4.026
INH9	−411.432	−6.167	−425.3754	591.826	5.112
INH10	−372.997	229.686	539.475	694.921	6.003
INH11	−794.901	79.312	689.978	1055.569	9.119
INH12	−901.872	−59.775	763.184	1182.960	10.219
INH13	−1102.43	−125.64	983.309	1266.215	10.939
INH14	−507.054	116.024	611.955	803.152	6.938
INH15	−847.898	−112.808	648.682	1073.519	9.274

Table 8: The static second hyperpolarizability (γ_{static}) of the studied compounds, calculated at $\omega = 0$ at the B3LYP-D/6-311G (d,p) level of theory in the gaseous phase.

Species	γ_{xxxx}	γ_{yyyy}	γ_{zzzz}	γ_{xxyy}	γ_{xxzz}	γ_{yyzz}	$\gamma_{total} \times 10^{-36}$ esu
INH	183239.00	3854.13	87083.70	2659.50	46066.80	2246.74	37.88
INH1	183722.00	5950.45	90823.40	4796.20	43941.60	3680.72	38.82
INH2	234874.00	20546.50	86508.80	24211.10	63646.40	11396.10	54.44
INH3	243315.00	25353.40	84023.10	32513.30	64149.10	12887.00	57.60
INH4	136059.00	10159.80	129249.00	9483.52	9483.52	7402.97	33.06
INH5	177961.00	3555.95	95850.10	2575.25	46702.20	1990.72	38.27
INH6	156375.00	4737.60	80935.10	4340.63	36334.50	2471.19	33.08
INH7	128524.00	4901.92	107463.00	4630.48	41328.60	4305.51	34.39
INH8	18477.20	7640.45	81610.20	9315.25	52669.30	5795.26	24.51
INH9	184301.00	8092.39	63934.30	13711.80	34270.20	9242.16	37.35
INH10	188585.00	7622.27	82806.50	7664.57	50002.10	4358.26	40.60
INH11	181608.00	7284.27	93479.20	5546.27	41470.20	2300.67	38.38
INH12	167395.00	4662.75	87287.70	3681.24	38448.40	3206.70	35.26
INH13	188566.00	5535.76	94775.70	5051.48	43980.60	3312.21	39.65
INH14	183228.00	4196.45	89054.40	4992.85	49023.70	2460.92	39.23
INH15	206706.00	8567.15	85354.20	9826.63	45110.50	3917.89	42.14

The molecular dipole moment is the basic property of a molecule, which is used to investigate intermolecular interactions. The higher the dipole moment, the stronger the intermolecular interactions and hence larger hyperpolarizabilities [55]. According to the results in Table 5, the computed dipole moment values of the investigated molecules range from 4.250 to 7.919 Debye. We note that INH13 and INH12 are characterized by the highest value of the total dipole moment; which are 7.919 and 7.541 Debye, respectively. These compounds, therefore, present good NLO responses.

Polarizability gives information on the distribution of electrons in the molecule and plays a fundamental role in determining the structure and orientation of a system [56]. The static isotropic ($\langle\alpha\rangle$) and anisotropic (Δ_α) polarizabilities of all the designed compounds are presented in Table 6.

Table 6 shows that the amplitudes of ($\langle\alpha\rangle$) and ((Δ_α)) of the N-(4-methoxybenzylidene) isonicotinohydrazone derivatives increase due to the presence of donor and acceptor substituents and the degree of π-conjugation in the system. Moreover, the static isotropic ($\langle\alpha\rangle$) polarizability values of the studied compounds increase as follows: INH < INH5 < INH12 < INH8 < INH13 < INH1 < INH9 < INH7 < INH11 < INH14 < INH10 < INH9 < INH4 < INH15 < INH3 < INH2. Among all the designed compounds, INH2 has the best isotropic polarizability value while INH has the least. The anisotropic (Δ_α) values follows the order: INH6 < INH12 < INH11 < INH7 < INH1 < INH9 < INH13 < INH < INH5 < INH8 < INH10 < INH4 < INH15 < INH14 < INH3 < INH2. Among all the designed compounds, INH2 also shows the best anisotropic polarizability value. Moreover, the great difference between the isotropic and anisotropic polarizability values of all the compounds shows that polarizability significantly depends on the direction of the applied electric field [47].

The first hyperpolarizabilities (second-order response) of the studied compounds are presented in Table 7.

In Table 7, the nonzero value of β_{static} shows that the investigated compounds possess first static hyperpolarizability. The first hyperpolarizability of urea (a prototype NLO molecule) was computed at the same level of theory ($\beta_{\text{static}} = 0.77 \times 10^{-30}$ esu). The predicted first hyperpolarizability of the studied compounds is much greater than that of urea and has NLO behaviours. Table 7 also presents the calculated values of the components of the first hyperpolarizability and the following order for β_{static} has been obtained: INH8 < INH9 < INH7 < INH6 < INH10 < INH2 < INH14 < INH11 < INH < INH15 < INH3 < INH1 < INH12 < INH5 < INH13 < INH4, indicating that INH5 and INH13 possess the highest NLO responses.

Presented in Table 8 are the second hyperpolarizabilities (third-order response) of the studied compounds.

The second hyperpolarizability of para-nitroaniline (reference molecule for the second hyperpolarizability) was computed at the same level of theory ($\gamma_{\text{static}} = 7.615 \times 10^{-36}$ esu) and compared to those of the studied compounds. The results show that all the studied compounds have second hyperpolarizability values much greater than that of PNA, implying they have good NLO responses. From Table 8, the second hyperpolarizability (γ_{static}) increases as follows: INH8 < INH4 < INH6 < INH7 < INH12 < INH9 < INH < INH5 < INH11 < INH1 < INH14 < INH13 < INH10 < INH15 < INH2 < INH3. The results also show that the size of the pi-conjugated bridge has a significant effect on the third-NLO response. Among all the designed compounds, INH2 and INH3 possess the best second hyperpolarizability values (i.e., 54.44×10^{-36} and 57.60×10^{-36} esu, respectively.

4. Conclusion

DFT and TD-DFT methods have been used to report a theoretical analysis of the charge transport and nonlinear optical properties of novel N-(4-methoxybenzylidene) isonicotinohydrazone derivatives. The reorganization energies of the electron ($\lambda_{\text{electron}}$) and hole ($\lambda_{\text{hole}}$), charge transfer integral of the electron (t_{electron}) and hole (t_{hole}), mobility of the electron (μ_{electron}) and hole (μ_{hole}), first hyperpolarizability (β_{static}), and static isotropic second hyperpolarizability (γ) have been discussed. Frontier molecular orbitals indicate that INH8 is the most reactive, and the band gaps of all the studied compounds are in the range of 3.933 to 4.645 eV. Calculated reorganization energy values indicate that the investigated compounds are electron transport materials. The low values of the reorganization energies reveal that compounds INH3 and INH9, can be considered as moderate electron transport materials with charge mobilities of 3.518×10^{-2} and $8.004 \times 10^{-2}\,\text{cm}^2\text{V}^{-1}\text{s}^{-1}$, respectively. In the same vein, the low reorganization energy of the hole reveals that compounds INH4 and INH15 can be considered as moderate hole transport materials. NLO investigations portray that compounds INH2 and INH3 exhibit higher values of static polarizability (isotropic and anisotropic) and second hyperpolarizability, while compounds INH4 and INH13 exhibit a larger value of first hyperpolarizability. The effect of donor/acceptor substituents and the π-conjugation system enhances the NLO and charge transport properties of the studied compounds. These findings are important for the design and applications of new molecules in optoelectronic engineering.

Data Availability

The data used to support the findings of this study are included within the article and in the supplementary data file.

Conflicts of Interest

The authors declare that they have no conflicts of interest.

Acknowledgments

The authors gratefully acknowledge the support for this project provided by the Cameroonian Ministry of Higher Education through the research modernization grants to lecturers of tertiary education.

Supplementary Materials

The supplementary material contains Tables and Figures as a part of this paper. Tables S1–S16 gives the optimized geometrical coordinates of the studied compounds, and Tables S17–S32 gives the optimized geometrical coordinates of the dimers. Figure S1 illustrates the optimized structures of the studied compounds, and Figure S2 illustrates the UV-Vis spectra of the studied compounds. (*Supplementary Materials*)

References

[1] C. I. L. Alongamo, S. N. Tasheh, N. K. Nkungli, F. K. Bine, and J. N. Ghogomu, "Structural, electronic, and charge transport properties of new materials based on 2-(5-mercapto-1, 3, 4-oxadiazol-2-yl)phenol for organic solar cells and light emitting diodes by DFT and TD-DFT," *Journal of Chemistry*, vol. 2022, Article ID 1802826, 15 pages, 2022.

[2] A. Mondal, L. Paterson, J. Cho et al., "Molecular library of OLED host materials-evaluating the multiscale simulation workflow," *Chemical Physics Reviews*, vol. 2, no. 3, Article ID 031304, 2021.

[3] F. Abbas, T. Nasir, M. Awais Ahmad et al., "TD-DFT study of small organic molecules based on boron subphthalocyanines by modifying axial substituents for organic photovoltaics," *International Journal of Scientific and Research Publications (IJSRP)*, vol. 11, no. 3, pp. 372-373, 2021.

[4] Y. Zhang, X. Cai, Y. Bian, X. Li, and J. Jiang, "Heteroatom substitution of oligothienoacenes: from good p-type semiconductors to good ambipolar semiconductors for organic field-effect transistors," *Journal of Physical Chemistry C*, vol. 112, no. 13, pp. 5148–5159, 2008.

[5] L. Kara Zaitri and S. M. Mekelleche, "DFT and TD-DFT study on quadratic NLO response and optoelectronic activity in novel Y-Shaped imidazole-based push-pull chromophores," *Journal of Molecular Modeling*, vol. 27, no. 5, 136 pages, 2021.

[6] C. B. Nwamba Tessa, A. D. Tamafo Fouegue, J. H. Nono, ·F. K. Bine, and J. N. Ghogomu, "DFT investigation on the effect of the permutation of some electron donating and accepting groups in the charge transfer process within 2-((E)-[2-hydroxyphenyl)imino] methyl)phenol," *Theoretical Chemistry Accounts*, vol. 141, no. 7, p. 31, 2022.

[7] N. S. Tasheh, N. K. Nkungli, and J. N. Ghogomu, "A DFT and TD-DFT study of ESIPT-mediated NLO switching and UV absorption by 2-(2′-hydroxy-5′-methylphenyl)benzotriazole," *Theoretical Chemistry Accounts*, vol. 138, no. 8, 100 pages, 2019.

[8] F. K. Bine, N. S. Tasheh, and J. N. Ghogomu, "A quantum chemical screening of two imidazole-chalcone hybrid ligands and their Pd, Pt and Zn complexes for charge transport and nonlinear optical (NLO) properties: a DFT study," *Computational Chemistry*, vol. 09, no. 04, pp. 215–237, 2021.

[9] M. Marinescu, "Synthesis and nonlinear optical studies on organic compounds in laser- deposited films," *Applied Surface of Science*, Intech Open, London, UK, 2018.

[10] A. Karakas, Y. Ceylan, M. Karakaya et al., "Theoretical diagnostics of second and third-order hyperpolarizabilities of several acid derivatives," *Open Chemistry*, vol. 17, no. 1, pp. 151–156, 2019.

[11] G. W. Ejuh, F. Tchangnwa Nya, N. Djongyang, and J. M. B. Ndjaka, "Theoretical study on the electronic, optoelectronic, linear and nonlinear optical properties and UV-Vis Spectrum of Coronene and Coronene substituted with Chlorine," *SN Applied Sciences*, vol. 2, no. 7, 1247 pages, 2020.

[12] S. Semin, X. Li, Y. Duan, and T. Rasing, "Nonlinear optical properties and applications of fluorenone molecular materials," *Advanced Optical Materials*, vol. 9, no. 23, Article ID 2100327, 2021.

[13] A. Üngördü, "Charge transfer properties of Gaq3 and its derivatives: an OLED study," *Chemical Physics Letters*, vol. 733, Article ID 136696, 2019.

[14] P. Reiser, M. Konrad, A. Fediai, S. Léon, W. Wenzel, and P. Friederich, "Analyzing dynamical disorder for charge transport in organic semiconductors via machine learning," *Journal of Chemical Theory and Computation*, vol. 17, no. 6, pp. 3750–3759, 2021.

[15] Y. Watanabe, H. Sasabe, and J. Kido, "Review of molecular engineering for horizontal molecular orientation in organic light-emitting devices," *Bulletin of the Chemical Society of Japan*, vol. 92, no. 3, pp. 716–728, 2019.

[16] X.-Q. Sun, G.-Y. Qin, P.-P. Lin et al., "Theoretical investigations on the charge transport properties of anthracene derivatives with aryl substituents at the 2, 6-position-thermally stable "herringbone" stacking motifs," *Physical Chemistry Chemical Physics*, vol. 23, no. 22, pp. 12679–12691, 2021.

[17] M. D. Halls and H. B. Schlegel, "Molecular orbital study of the first excited state of the OLED material tris(8-hydroxyquinoline)aluminum(III)," *Chemistry of Materials*, vol. 13, no. 8, pp. 2632–2640, 2001.

[18] W. G. Quirino, C. Legnani, M. Cremona et al., "Photoluminescence, photoabsorption and photoemission studies of hydrazone thin film used as hole transporting material in OLEDs," *Journal of the Brazilian Chemical Society*, vol. 19, no. 5, pp. 872–876, 2008.

[19] K. Naseema, K. V. Sujith, K. B. Manjunatha, B. Kalluraya, G. Umesh, and V. Rao, "Synthesis, characterization and studies on the nonlinear optical parameters of hydrazones," *Optics & Laser Technology*, vol. 42, no. 5, pp. 741–748, 2010.

[20] R. S. Moraes, R. E. Aderne, M. Cremona, and N. A. Rey, "Luminescent properties of a di-hydrazone derived from the antituberculosis agent isoniazid: potentiality as an emitting layer constituent for OLED fabrication," *Optical Materials*, vol. 52, pp. 186–191, 2016.

[21] F. Z. Henari and P. S. Patil, "Nonlinear optical properties and optical limiting measurements of {(1z)-[4-(dimethylamino) phenyl]methylene} 4-nitrobenzocarboxy hydrazone monohydrate under CW laser regime," *Optics and Photonics Journal*, vol. 04, no. 07, pp. 182–188, 2014.

[22] Y. Yao, H.-L. Xu, Y.-Q. Qiu, and Z.-M. Su, "The second-order nonlinear optical property of hydrazones-based photochromic complexes: a DFT study," *Journal of Molecular Liquids*, vol. 327, Article ID 114882, 2021.

[23] N. Boukabcha, A. Djafri, Y. Megrouss et al., "Synthesis, crystal structure, spectroscopic characterization and nonlinear optical properties of (Z)-N′-(2, 4-dinitrobenzylidene)-2-(quinolin-8-yloxy)acetohydrazide," *Journal of Molecular Structure*, vol. 1194, pp. 112–123, 2019.

[24] M. Kudrat-E-Zahan and M. M. Haque, "Synthesis, characterization and biological activity studies of mixed ligand complexes with Schiff base and 2, 2′-bipyridine," *International Journal of Applied Sciences*, vol. 6, pp. 1–7, 2019.

[25] C. T. Tedjeuguim, S. N. Tasheh, C. I. L. Alongamo, and J. N. Ghogomu, "A DFT and TD-DFT study of charge transport and non-linear optical properties of N-(4-methoxybenzylidene)isonicotinohydrazone, 2, 2′-bipyridine and their Fe^{2+}, Ni^{2+}, Cu^{2+}, Pd^{2+} and Pt^{2+} complexes," *Journal of Chemical Sciences*, vol. 134, no. 3, pp. 70–15, 2022.

[26] M. Frisch, G. Trucks, and H. Schlegel, *Gaussian09*, Gaussian Inc, Wallingford, CT, USA, 2009.

[27] R. Dennington, T. A. Keith, and J. M. Millam, *Gauss View 6.0.1*, Semi chem Inc, Shawnee Mission, Kansas, 2016.

[28] E. Lewars, *Computational Chemistry: Introduction to the Theory and Applications of Molecular and Quantum Mechanics*, Klumer Academy Publishers, New York, NY, USA, 2003.

[29] S. Grimme, J. Antony, S. Ehrlich, and H. Krieg, "A consistent and accurate ab initio parametrization of density functional dispersion correction (DFT-D) for the 94 elements H-Pu," *The Journal of Chemical Physics*, vol. 132, no. 15, Article ID 154104, 2010.

[30] R. Ditchfield, W. J. Hehre, and J. A. Pople, "Self-consistent molecular orbital methods: an extended Gaussian-type basis for molecular orbital studies of organic molecules," *The Journal of Chemical Physics*, vol. 54, no. 2, pp. 724–728, 1971.

[31] M. Naganathappa, S. Ravula, B. Kolli, and A. Chaudhari, "Nonlinear optical properties and spectroscopic characterization of Y-shaped polymer using quantum chemical approach," *Journal of Molecular Modeling*, vol. 26, no. 11, 299 pages, 2020.

[32] T. Yanai, D. P. Tew, and N. C. Handy, "A new hybrid exchange-correlation functional using the coulomb-attenuating method (CAM-B3LYP)," *Chemical Physics Letters*, vol. 393, no. 1-3, pp. 51–57, 2004.

[33] M. J. S. Dewar and W. Thiel, "Ground states of molecules. 38. The MNDO method. Approximations and parameters," *Journal of the American Chemical Society*, vol. 99, no. 15, pp. 4899–4907, 1977.

[34] Z. Chen, Z. He, Y. Xu, and W. Yu, "Density functional theory calculations of charge transport properties of "plate-like" coronene topological structures," *Journal of Chemical Sciences*, vol. 129, no. 9, pp. 1341–1347, 2017.

[35] T. P. Nguyen, P. Roy, and J. H. T. Shim, "Remarkable charge-transfer mobility from [6]to [10]phenacene as a high performance p-type organic semiconductor," *Physical Chemistry Chemical Physics*, vol. 20, no. 13, pp. 8658–8667, 2018.

[36] R. A. Marcus, "Chemical and electrochemical electron-transfer theory," *Annual Review of Physical Chemistry*, vol. 15, no. 1, pp. 155–196, 1964.

[37] F. May, M. Al-Helwi, B. Baumeier et al., "Design rules for charge-transport efficient host materials for phosphorescent organic light-emitting diodes," *Journal of the American Chemical Society*, vol. 134, no. 33, pp. 13818–13822, 2012.

[38] M. Qiu, W. Pei, Q. Lu, Z. Li, Y. Li, and J. Liang, "DFT characteristics of charge transport in DBTP-based hole transport materials," *Applied Sciences*, vol. 9, no. 11, 2244 pages, 2019.

[39] F. Sun and R. Jin, "DFT and TD-DFT study on the optical and electronic properties of derivatives of 1, 4-bis(2-substituted-1, 3, 4-oxadiazole)benzene," *Arabian Journal of Chemistry*, vol. 10, pp. 2988–2993, 2017.

[40] K. Buldurun, E. Tanis, N. Turan, N. Çolak, and N. Çankaya, "Solvent effects on the electronic and optical properties of Ni(II), Zn(II), and Fe(II) complexes of a Schiff base derived from 5-bromo-2-hydroxybenzaldehyde," *Journal of Chemical Research*, vol. 45, no. 7-8, pp. 753–759, 2021.

[41] R. Jin, X. Zhang, and W. Xiao, "Theoretical studies of photophysical properties of D-π-A-π-D-type diketopyrrolopyrrole-based molecules for organic light-emitting diodes and organic solar cells," *Molecules*, vol. 25, no. 3, 667 pages, 2020.

[42] H. H. Khalid, S. Erkan, and N. Bulut, "Halogens effect on spectroscopy, anticancer and molecular docking studies for platinum complexes," *Optik*, vol. 244, Article ID 166324, 2021.

[43] W. Q. Deng and W. A. Goddard, "Predictions of hole mobilities in oligoacene organic semiconductors from quantum mechanical calculations," *The Journal of Physical Chemistry B*, vol. 108, no. 25, pp. 8614–8621, 2004.

[44] A. Irfan, A. G. Al-Sehemi, A. R. Chaudhry, and S. Muhammad, "The structural, electro-optical, charge transport and nonlinear optical properties of oxazole(4Z)-4-Benzylidene-2-(4-methylphenyl)-1, 3-oxazol-5(4H)-one derivative," *Journal of King Saud University Science*, vol. 30, no. 1, pp. 75–82, 2018.

[45] H. A. Kurtz, J. J. P. Stewart, and K. M. Dieter, "Calculation of the nonlinear optical properties of molecules," *Journal of Computational Chemistry*, vol. 11, no. 1, pp. 82–87, 1990.

[46] V. S. Naik, P. S. Patil, Q. A. Wong, C. K. Quah, N. B. Gummagol, and H. S. Jayanna, "Molecular structure, linear optical, second and third-order nonlinear optical properties of two non-centrosymmetric thiophene-chalcone derivatives," *Journal of Molecular Structure*, vol. 1222, Article ID 128901, 2020.

[47] B. Ali, M. Khalid, S. Asim et al., "Key electronic, linear and nonlinear optical properties of designed disubstituted quinoline with carbazole compounds," *Molecules*, vol. 26, no. 9, 2760 pages, 2021.

[48] E. S. Mirkamali and R. Ahmadi, "Adsorption of melphalan anticancer drug on the surface of boron nitride cage ($B_{12}N_{12}$): a comprehensive DFT study," *Journal of Medicinal Chemistry Science*, vol. 3, pp. 199–207, 2020.

[49] B. Nosheen, F. Perveen, Z. Ashraf, A. Bais, and T. Noor, "Charge transfer and opto-electronic properties of some newly designed polycatenar discotic liquid crystal derivatives: a DFT study," *Journal of Molecular Modeling*, vol. 26, no. 10, p. 291, 2020.

[50] M. R. Albayati, S. Kansız, N. Dege et al., "Synthesis, crystal structure, hirshfeld surface analysis and DFT calculations of 2-[(2, 3 dimethylphenyl) amino]-N′-[(E)-thiophen-2-ylmethylidene]benzohydrazide," *Journal of Molecular Structure*, vol. 1205, Article ID 127654, 2020.

[51] Y. Oueslati, S. Kansız, A. Valkonen, T. Sahbani, N. Dege, and W. Smirani, "Synthesis, crystal structure, DFT calculations, hirshfeld surface, vibrational and optical properties of a novel hybrid non-centrosymmetric material (C10H15N2) 2H2P2O7," *Journal of Molecular Structure*, vol. 1196, pp. 499–507, 2019.

[52] G. Demirtaş, N. Dege, H. İçbudak, Ö. Yurdakul, and O. Büyükgüngör, "Experimental and DFT studies on Poly [di-μ3-acesulfamato-O, O: O′; O′: O, O-di-μ-acesulfamato-O, O; N-di-μ-aqua-dicalcium (II)] complex," *Journal of Inorganic and Organometallic Polymers and Materials*, vol. 22, no. 4, pp. 671–679, 2012.

[53] A. H. Pandith and N. Islam, "Electron transport and nonlinear optical proper-ties of substituted aryl dimesityl boranes: a DFT Study," *PLoS One*, vol. 9, no. 12, Article ID 114125, 2014.

[54] V. M. Vidya, S. Pola, and P. Chetti, "Optoelectronic and charge transport properties of D-n-A type1, 3, 5-triazine derivatives: a combined experimental and DFT study," *Spectrochimica Acta Part A: Molecular and Biomolecular Spectroscopy*, vol. 245, Article ID 118940, 2021.

[55] S. R. Maidur, P. S. S. Patil, S. V. Rao, M. Shkir, and S. M. Dharmaprakash, "Experimental and computational studies on second-and third-order nonlinear optical properties of a novel D-π-A type chalcone derivative: 3-(4-methoxyphenyl)-1-(4-nitrophenyl) prop-2-en-1-one," *Optics & Laser Technology*, vol. 97, pp. 219–228, 2017.

[56] C. D. D. Mveme, F. Tchangnwa Nya, G. W. Ejuh, R. A. Yossa Kamsi, and J. M. B. Ndjaka, "Density functional theory study of optoelectronic, nonlinear optical, piezoelectric and thermodynamic properties of poly (3, 4-ethylenedioxythiophene), poly(3, 4-ethylenedioxyselenophene) and their derivatives," *Optical and Quantum Electronics*, vol. 52, no. 8, 373 pages, 2020.